OncoTargets and Therapy

Dovepress
open access to scientific and medical research

Open Access Full Text Article

ORIGINAL RESEARCH

Dual-Mode Contrast Agents with RGD-Modified Polymer for Tumour-Targeted US/NIRF Imaging

This article was published in the following Dove Press journal:
OncoTargets and Therapy

Zhenhui Nie[1,*]
Ningbin Luo[1,*]
Junjie Liu[2]
Yu Zhang[1]
Xinyi Zeng[1]
Danke Su[1]

[1]Department of Radiology, Affiliated Tumour Hospital of Guangxi Medical University, Nanning, Guangxi, People's Republic of China; [2]Department of Medical Ultrasound, Affiliated Tumour Hospital of Guangxi Medical University, Nanning, Guangxi, People's Republic of China

*These authors contributed equally to this work

Background: Cancer diagnosis and treatment during the early stages of disease remain extremely challenging clinical tasks. The development of effective multimode contrast agents could greatly facilitate the early detection of cancer.

Materials and Methods: We prepared dual-mode contrast agents using a biotin/avidin bioamplification system. Through in vivo and in vitro experiments, we verified the imaging performance of this contrast agents in both fluorescence and ultrasound and its targeting specificity for MDA-MB-231 cells.

Results: The RGD peptide-labelled microbubbles showed excellent targeting of αvβ3 integrin expressed by MDA-MB-231 cells in vitro and in vivo. The signal intensity and time duration of ultrasound imaging using these particles were superior to those obtained with a typical ultrasound contrast agent in the clinic. The tumour areas also demonstrated high Cy5.5 accumulation by fluorescence imaging.

Conclusion: The results show that this targeted dual-mode imaging system yields outstanding US/NIRF imaging results, possibly allowing the early clinical diagnosis of cancer.

Keywords: ultrasound, molecular imaging, microbubble, targeting imaging

Introduction

Targeted ultrasound molecular imaging is a valuable tool that is being increasingly adapted for clinical applications.[1–3] Conventional ultrasound contrast agents (UCAs) are typically gas-filled microbubbles (MBs) containing a perfluorinated gas in a thin lipid monolayer shell.[4–6] UCAs are delivered through blood vessels; thus, their size is limited to the diameter of capillaries.[7] Most studies report that these particles have an average diameter of ~1.5–4 μm, which allows the microbubbles to be well dispersed within the liquid and to produce an acoustic scattering signal that is sufficient for effective imaging within several centimetres of tissue depth.[8–10] In contrast to expensive and time-consuming CT, MRI or PET clinical examinations, patients can be administered microbubbles at the bedside, and the microbubbles allow the precise localization of lesions within a few minutes of administration to guide biopsies, ablation or rapid diagnosis.[11–13] However, the low sensitivity of ultrasound molecular imaging limits the early detection of lesions, which is closely related to the survival rate of cancer patients.[14–16] The features of near-infrared fluorescence (NIRF), including its deep tissue penetration, low background fluorescence interference and low biotoxicity, can overcome the limitations of ultrasound. Using optical imaging technology, it is possible to precisely visualize tumours in vivo and in vitro.[17–20]

Correspondence: Danke Su
Email sudanke@gxmu.edu.cn

submit your manuscript | www.dovepress.com
DovePress
http://doi.org/10.2147/OTT.S256044

αvβ3 integrin is highly expressed within the cytoplasm of various tumour cells and neovascular endothelial cells, and it plays an important role in tumour angiogenesis, invasion and metastasis.[21,22] The specifically labelled exogenous RGD peptide binds to the integrin αVβ3 site after entering the body and thus could be used as an indicator that reaches the tumour tissue for visualization by various imaging methods.[23–25] In addition, the selectivity of αVβ3 integrin targeting microbubbles to angiogenic endothelium can be used to monitor tumour development.[26–28]

To improve the application potential of these novel microbubbles, we designed a biotin/avidin bioamplification system to prepare US/NIRF dual-mode targeting microbubbles.[29–32] The targeting system actualizes a combination of high specific uptake in tumours and low retention in normal tissues, leading to good imaging results (see Figure 1). This article describes 1) the preparation of dual-modal targeted RGD-Cy5.5-MBs and their performance in vitro and 2) the evaluation of the US/fluorescent imaging capabilities of RGD-Cy5.5-MBs within tumour areas in tumour-bearing mouse models.

Materials and Methods

Preparation of RGD-Cy5.5-MBs

First, RGDfk antibody powder (GenicBio BioTech Co. Ltd., Shanghai, China) was dissolved in 1x PBS to a concentration of 2.0 mg/mL, and the solution was adjusted to pH 8.3–8.5 with 1 M NaHCO3 (Xian Ruixi Biological Technology Co. Ltd., Henan, China). Twenty-seven microlitres of biotin (Thermo Scientific, USA) was slowly added to 2 mL of RGDfk solution. Then, 1.0 mg of Sulfo-Cyanine 5.5 NHS ester (Xian Ruixi Biological Technology Co. Ltd., Xian, China) was dissolved in 180 μL of DMSO (Solarbio Company, Beijing, China) to a concentration of 5.5 mg/mL, and 90 μL of this solution was slowly added to 2 mL of RGDfk solution. The mixture was stirred at room temperature for 5 h and protected from light. After the reaction was completed, the above solution was subjected to ultrafiltration washings with 1× PBS overnight, and the RGD-Cy5.5 solution preparation was finished. Next, the USphereTM Labeler ultrasonic microbubble contrast agent (TRUST Biosonics Inc., Zhubei City, Hsinchu County) was activated

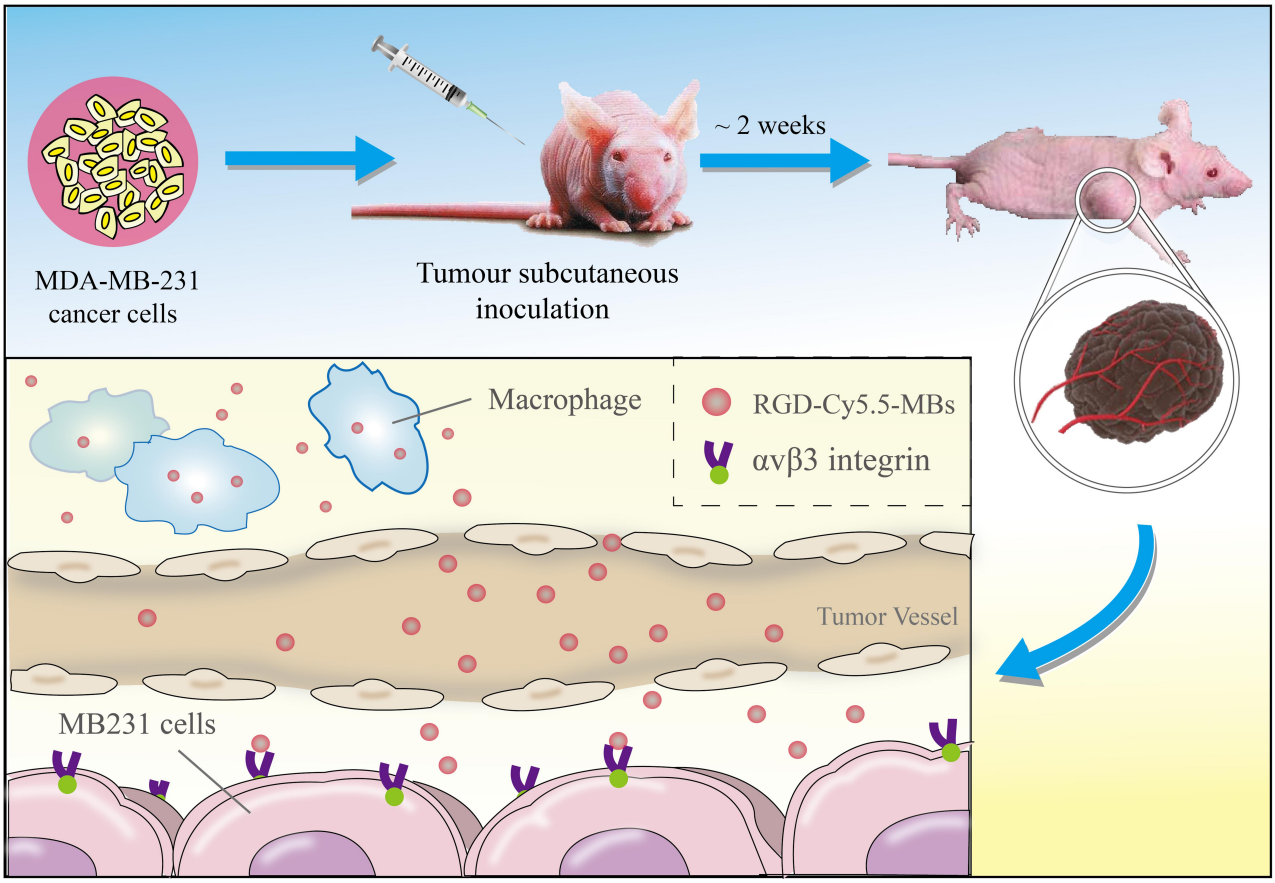

Figure 1 Schematic illustration of in-situ imaging and targeted binding mechanism of RGD-Cy5.5-MBs. **Abbreviations:** RGD, arginine–glycine–aspartate; MB, microbubble.

by UltraMix™ (TRUST Bio-sonics Inc., Zhubei City, Hsinchu County) via a 40 second rapid shock. Then, 1.0 nmol of RGD-Cy5.5 solution was added to the microbubble solution and thoroughly mixed with a vortex oscillator (Qilinbeier Co. Ltd., Haimen, China). The mixed solution was incubated at 4°C for a 15-minute reaction. Finally, the solution of RGD-Cy 5.5-MBs was resuspended in 0.9 mL of deionized water and stored at 4°C.

Characterization of RGD-Cy5.5-MBs

The size distribution and zeta potential were determined by a particle analyser (Beckman, USA), and these results were applied to further enhance the properties of the RGD-Cy5.5-MBs. Notably, zeta potential was determined in PBS solution. All measurements were performed 3 times, and representative images are shown. Fluorescent images were acquired by using a confocal microscope (Nikon, Japan) and analysed by ImageJ software.

Cellular Uptake Study in vitro

Human MDA-MB-231 breast cancer cells were provided by the Stem Cell Bank, Chinese Academy of Sciences and were maintained in DMEM with 5% FBS and 1% penicillin-streptomycin at 37°C with 5% CO_2. For the cellular uptake study, MDA-MB-231 cells were cultured in 35 mm glass-bottom culture dishes (MatTek, USA) with $2x10^4$ cells mL^{-1} for 24 h. The medium was then replaced by a new medium containing free RGD-Cy5.5-MBs or nontargeted MBs. After 2 h of incubation, the cells were washed three times with PBS and fixed with 4% paraformaldehyde for 20 minutes. DAPI was used to stain the nuclei for 5 minutes. Fluorescence images were acquired by confocal laser scanning microscopy (TCS SP8, Leica, Germany).

Cellular Toxicity Study in vitro

The cellular toxicity of RGD-Cy5.5-MBs in vitro was verified by a Cell Counting Kit-8 (CCK8) viability assay. MDA-MB-231 cells were cultured in 96-well plates at $2x10^3$ cells mL^{-1} for 24 h. Then, the cells were treated with 0.1 mL of RGD-Cy5.5-MBs at MB concentrations of 106, 107, 108 and 109 mL^{-1}. Sonovue at the same concentrations was applied as a control. After incubation for 24 h, 10 μL of CCK8 solution was added to each well, and the cells were further incubated for 1 h. A microplate reader (Thermo Scientific, USA) was used to evaluate the optical absorbance of each well at 450 nm.

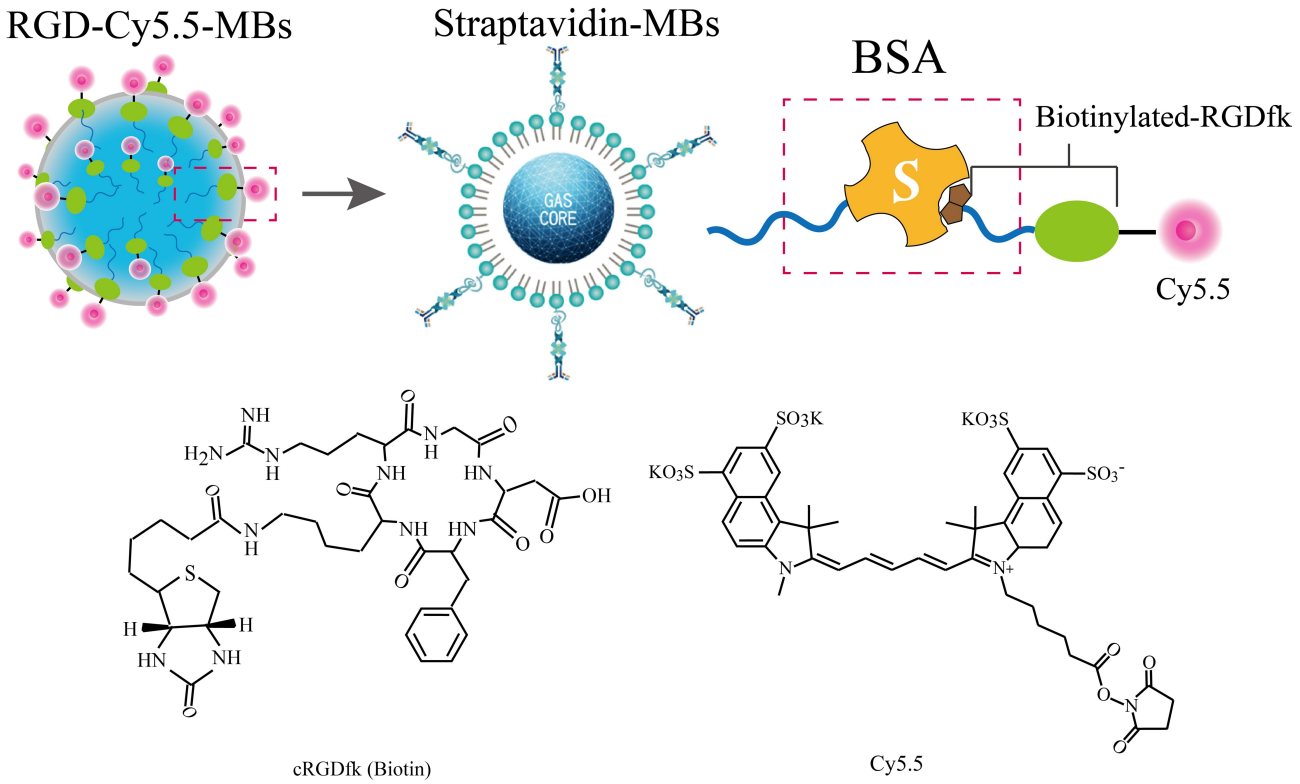

Figure 2 The detailed diagrams of the composition in Biotin-Avidin System-based RGD-Cy5.5- MBs. **Abbreviations:** RGD, arginine–glycine–aspartate; MB, microbubble.

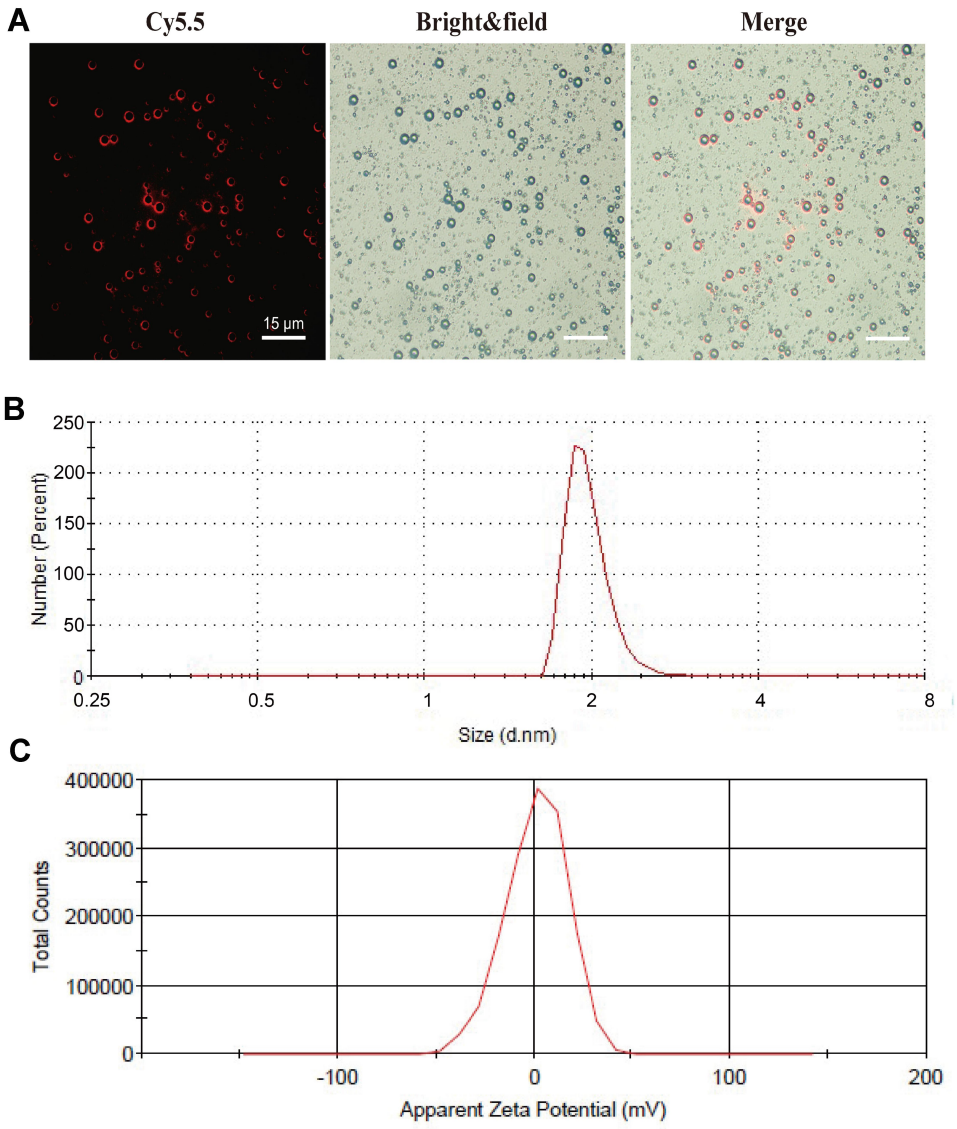

Figure 3 Optical microscope images (**A**) Size distributions (**B**) Zeta potential (**C**) of RGD-Cy5.5- MBs (scale bar: 15 μm). **Abbreviations:** RGD, arginine–glycine–aspartate; MB, microbubble.

Ultrasound Imaging in vitro

First, MDA-MB-231 cells were cultured in 6-well plates at $3x10^5$ cells mL^{-1} and allowed to grow for 24 h. Then, 0.2 mL of RGD-Cy5.5-MBs with concentrations of $2x10^8$ mL^{-1} and $2x10^7$ mL^{-1} were added to the wells and incubated with cells for 2 h. PBS solution was used as a blank control. Then, the cells were harvested by 0.05% trypsin EDTA and resuspended in PBS. The solutions were added to agarose gel. Ultrasound images were acquired by a Vevo 2100 (Fujifilm Visual Sonics Inc., Canada) ultrasound system using a high-frequency linear transducer (7 MHz, mechanical index [MI] 0.09, dynamic range 50 dB).

Animal Tumour Model

All 4-week-old BALB/c mice were purchased from the Laboratory Animal Center of Guangdong Province, and the animal experiments were approved by Guangxi Medical University Laboratory Animal Center. Animal ethics review follows the Guiding Opinions on the Treatment of Laboratory Animals issued by the Ministry of Science and Technology of the People's Republic of China and the Laboratory Animal-Guideline for Ethical Review of Animal Welfare issued by the National Standard GB/T35892-2018 of the People's Republic of China. The right flanks of BALB/c mice were subcutaneously injected with MDA-MB-231 cells ($2x10^6$ cells in

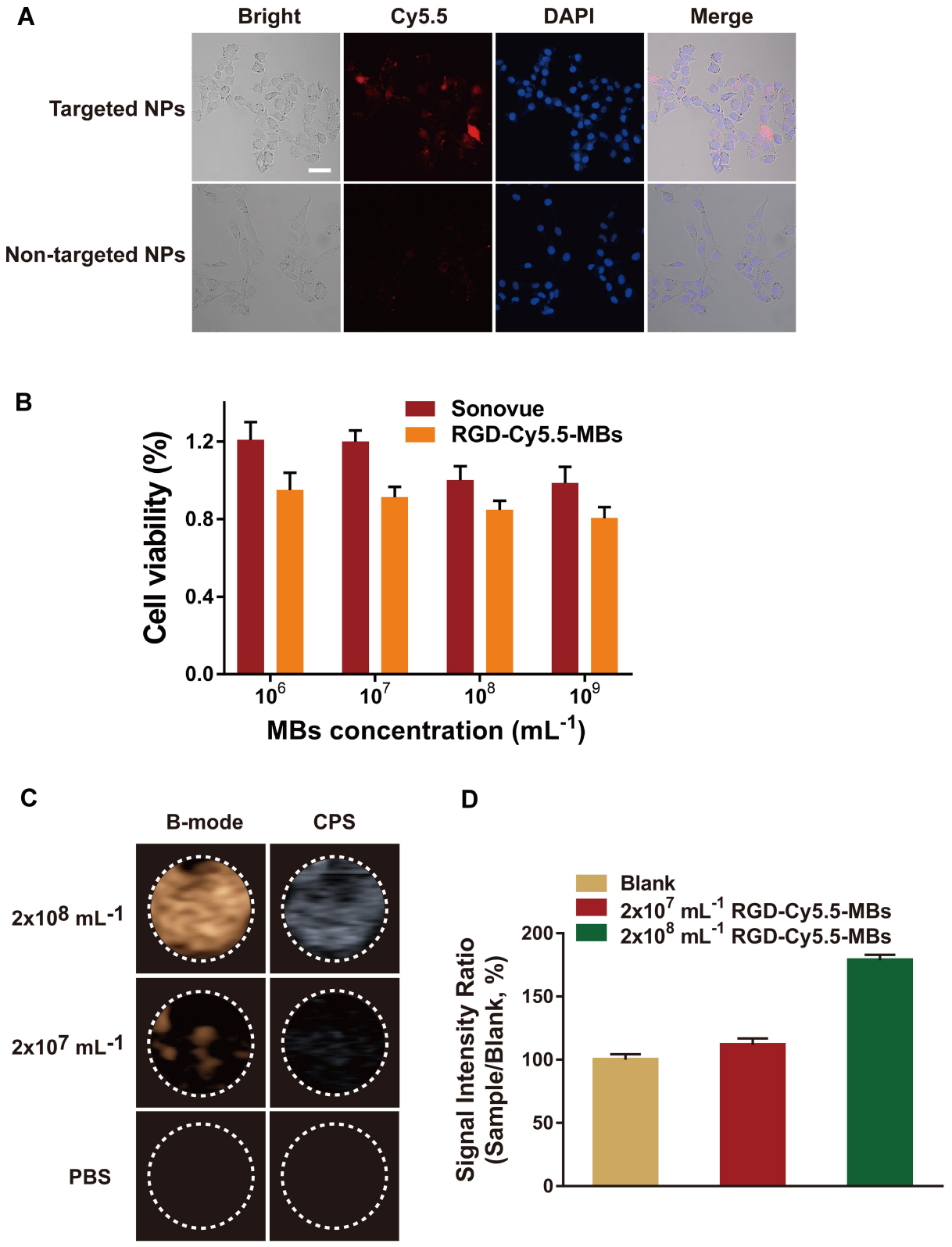

Figure 4 (**A**) Confocal fluorescence images of MB231 cells incubated with RGD-Cy5.5-MBs and non-targeted MBs (scale bar: 50 μm). (**B**) Cells viability of MB231 cells respectively incubated with RGD-Cy5.5- MBs and Sonovue in different concentrations. (**C**) Ultrasound contrast images of MB231 cells treated with RGD-Cy5.5-MBs in MBs concentrations of $2x10^8$ and $2x10^7$ mL^{-1}, PBS as a control. (**D**) Signal Intensity Rate is calculated by sample/blank, sample represents the ultrasound echo intensity of RGD-Cy5.5-MBs, blank represents the ultrasound echo intensity of PBS.

Abbreviations: MB231, breast cancer cells; RGD, arginine–glycine–aspartate; MB, microbubble; PBS, phosphate buffered saline.

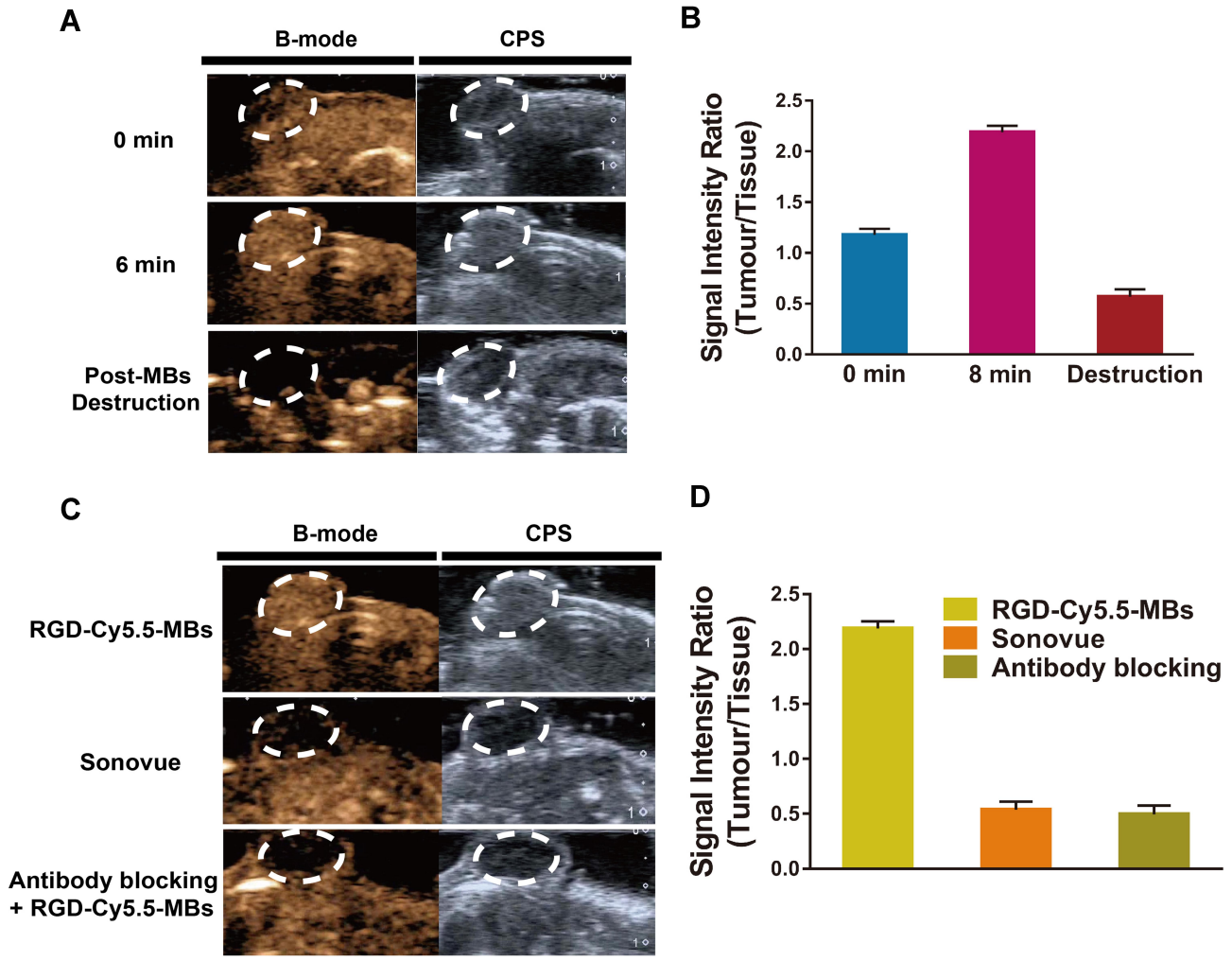

Figure 5 (**A**) Ultrasound imaging of tumors in vivo at different time after injection of RGD-Cy5.5-MBs. (**B**) Echo intensity rate as a function of time is calculated by tumor/tissue, tumor represents the echo intensity of the tumor area, tissue represents the echo intensity of the tissue around tumors. (**C**) Ultrasound imaging of tumors after respectively injection of RGD-Cy5.5-MBs, Sonovue and the group of antibody blocking at 6 min. (**D**) Echo intensity rate in tumor/tissue of the three groups above. **Abbreviations:** RGD, arginine–glycine–aspartate; MB, microbubble.

200 μL per mouse). The tumours were allowed to grow for approximately 2 weeks before imaging.

Ultrasound Imaging in vivo

Mice were anaesthetized via 2% isoflurane, and their bodies were fixed on a heated pad to maintain body temperature at 37° C. RGD-Cy5.5-MBs ($2x10^8$ mL^{-1}, 0.2 mL) were injected into the mice via the tail vein. Ultrasound examinations were performed using an Aplio 500 (Toshiba Corporation, Japanese) and a 7-MHz transducer. Images were acquired in B-mode and CEUS-mode. The acoustic focus zone was placed at the centre of the tumour with the largest cross-section, and the tissues adjacent to the tumour were also imaged. At the end of imaging, a high-power destructive pulse (8.0 MHz, MI 1.8) was applied to destroy all microbubbles in the tumour area. The same amount of Sonovue (Bracco International B.V., Switzerland) was injected into mice to serve as a control. Mice pre-treated with αv-integrin antibody were examined to verify the targeting of RGD-Cy5.5-MBs.

Fluorescence Imaging in vivo

RGD-Cy5.5-MBs were added into Eppendorf tubes and processed by ultrasound scanning using a high-frequency linear transducer (7 MHz, mechanical index 0.09), and then the fluorescence intensity was measured by a fluorescence imaging system. The groups with no ultrasound scanning and PBS were used as controls.

A total of 200 μL of RGD-Cy5.5-MBs were injected via the tail vein for fluorescence imaging in vivo, and nontargeted MBs were used as a control. The FX PRO

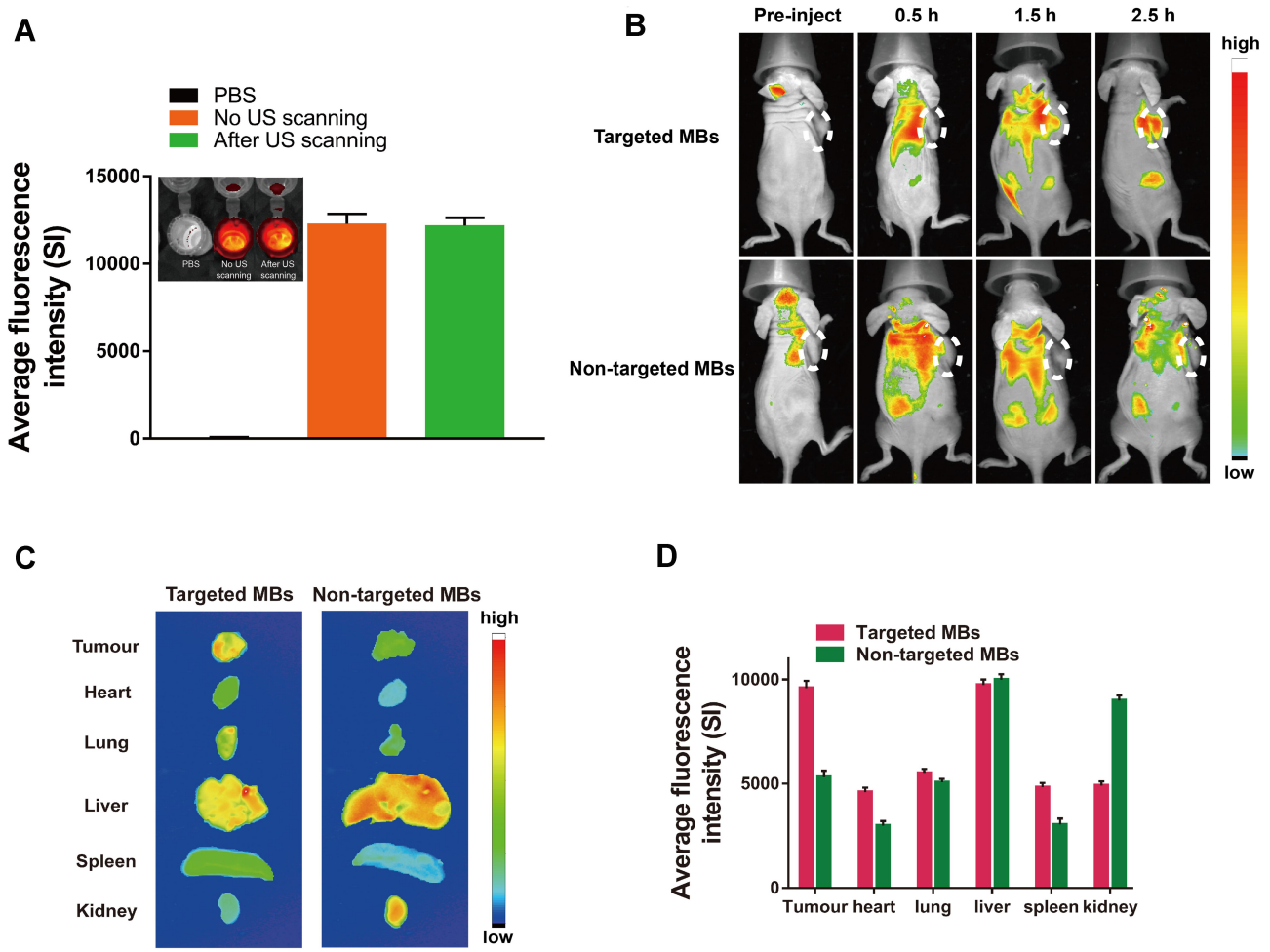

Figure 6 (**A**) Fluorescence imaging in vitro and averaged fluorescence intensity under ultrasound scanning and non-ultrasound scanning, PBS as a control. (**B**) Fluorescence imaging in vivo of mice at pre-injection and post-injection after injection of RGD-Cy5.5-MBs and non-targeted MBs at 0.5, 1.5 and 2.5 hours. (**C**) The fluorescence images of tissues dissected from the mice. (**D**) Averaged fluorescence intensity of these tissues.
Abbreviations: RGD, arginine–glycine–aspartate; MB, microbubble; PBS, phosphate buffered saline.

in vivo fluorescence imaging system (Bruker, Switzerland) was used for scanning. Images of the mice were acquired prior to injection. Fluorescence scanning was then performed in 30-minute intervals to record the signal transitions of the tumours. The mice were sacrificed when the in vivo fluorescence signal was highly accumulated in the tumour area. The main organs and tumours were harvested for fluorescence scanning in vitro. Molecular imaging software (Bruker, Switzerland) was applied for quantitative analysis of the fluorescence intensity.

Tumour Immunofluorescence and HE Staining

The tissues of organs and tumours were fixed by OCT compound (Sakura Finetek, USA) and cut into frozen slices with a cryostat microtome (Leica, Heidelberg, Germany). The αv integrin was stained with rabbit monoclonal anti-integrin αv antibody (dilution 1:500, Abcam) and Alexa 488-conjugated goat anti-rabbit secondary antibody (dilution 1:1000, Abcam). The β3 integrin was subsequently stained with mouse monoclonal anti-integrin β3 antibody (dilution 1:500, Abcam) and Alexa 594-conjugated goat anti-mouse secondary antibody (dilution 1:1000, Abcam). Cell nuclei were stained with DAPI (Solarbio, Beijing, China). Images were obtained by confocal laser scanning microscopy (TCS SP8, Leica, Germany).

Results and Discussion

Characterization of RGD-Cy5.5-MBs

To ensure the biosafety of dual-mode contrast agents for application, the biotin-avidin system (BAS), which exhibits strong biostability, was employed to conjugate RGD-Cy5.5 to MBs to

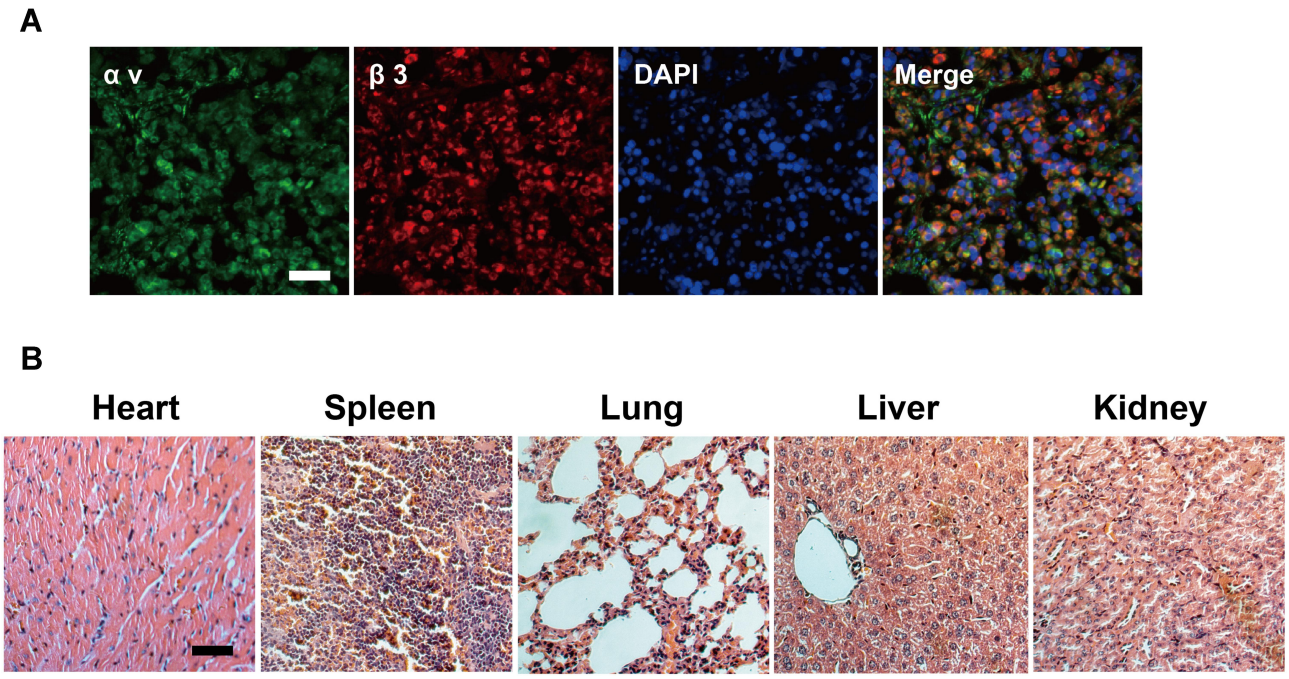

Figure 7 (**A**) Fluorescent imaging of tumor frozen sections from MDA-MB-231 cells–bearing mice injected with RGD-Cy5.5-MBs (scale bar: 50 μm). (**B**) H&E-stained organ slices collected from mice after injection of RGD-Cy5.5-MBs (scale bar: 50 μm).
Abbreviations: MDA-MB-231, breast cancer cells; RGD, arginine–glycine–aspartate; MB, microbubble; H&E, hematoxylin-eosin.

avoid degradation in the body. Biotin and avidin exhibit the greatest degree of noncovalent binding. The binding stability between biotin and avidin is strong, specific and not affected by reagent concentration, environmental pH or other organic solvents, such as protein denaturants. Furthermore, the RGD moiety conjugates with the MBs to realize specific targeted accumulation in the tumour area. Specifically, the RGDfk motif conjugates with the biotinylated antibody and links with Sulfo-Cyanine5.5 NHS ester by an amide reaction. Then, the RGD-Cy5.5 and avidin-labelled MBs form a globular biotin-avidin complex. The detailed synthesis procedure of RGD-Cy5.5-MBs is shown in Figure 2.

Optical microscopy images of RGD-Cy5.5-MBs show that the microbubbles were spherical, with clear outlines and uniform size in the field of view (see Figure 3A). In addition, the red fluorescence around the microbubbles indicates that Cy5.5 attached to the surface of the RGD-Cy5.5-MBs. Dynamic light scattering (DLS) analysis of RGD-Cy5.5-MBs (average 1789.9 nm; see Figure 3B) revealed narrow peaks. This is similar to the previous study concerning targeted RGD-MBs for Hep-2 tumour angiogenesis, demonstrating that the microbubbles were homogeneously dispersed.[33] The average polydispersity index was 1.504. Zeta potential was measured to confirm the surface charge (average −2.6 mV; see Figure 3C).

In vitro Experiments with RGD-Cy5.5-MBs

A confocal laser scanning microscope (CLSM) was used to view the cellular uptake of the RGD-Cy5.5-MBs (see Figure 4A). MDA-MB-231 cells treated with RGD-Cy5.5-MBs displayed obvious fluorescence enhancement. As a control, cells treated with nontargeted MBs showed minimal fluorescence in the cytoplasm, which indicated that the RGD-based targeting strategy was effective for enhancing the uptake of MBs by MDA-MB-231 cells.[24,34]

MDA-MB-231 cells were also used to investigate the biocompatibility of RGD-Cy5.5-MBs (see Figure 4B). In the range of MB concentrations, no significant decrease in MDA-MB-231 cell viability was observed. Sonovue is an ultrasound contrast agent that exhibits good biosafety and is widely used in clinical diagnosis.[35,36] The viability of cells in the experimental group was slightly lower than that of cells treated with Sonovue, although both were above 80%. The significantly lower cytotoxicity of RGD-Cy5.5-MBs according to the CCK8 results indicates their good biocompatibility.

In vitro targeted cell ultrasound imaging was performed to further verify both the special targeting property of the RGD-Cy5.5-MBs and its outstanding contrast in the US. Regarding the function of the MBs at a concentration of $2x10^8$ mL^{-1}, the

images in CEUS-mode of the treated MDA-MB-231 cells showed a significant signal increase (see Figure 4C). In addition, the signal of the cells treated with RGD-Cy5.5-MBs at an MB concentration of $2x10^7$ $mL^{-}1$ was much lower than that of the same cells treated with a concentration of $2x10^8$ mL^{-1}. The intensity of PBS served as a baseline, and the ultrasound intensity ratio of the cells treated with RGD-Cy5.5-MBs at $2x10^8$ mL^{-1} was even higher (see Figure 4D).

Ultrasound Contrast Imaging of RGD-Cy5.5-MBs

After injection of cRGD-Cy5.5-MBs through the tail vein, the ultrasound images showed significant contrast enhancement in the tumour tissues (see Figure 5A). The ultrasound intensity signal in the tumour reached the highest value at 6 minutes after injection. In addition, the lack of signals after microbubble destruction indicated that a high contrast-to-tissue ratio was achieved with cRGD-Cy5.5-MBs (see Figure 5B). When the peak intensity of the tumour after administration of cRGD-Cy5.5-MBs was reached, the tumour-to-tissue signal ratio was 4-fold higher than that observed by Sonovue administration. Furthermore, the specificity of cRGD-Cy5.5-MBs for αvβ3 integrin in the tumour endothelium was confirmed by pretreatment with αv-integrin antibody (see Figure 5C). The tumour-to-tissue signal ratio produced by cRGD-Cy5.5-MBs was reduced by 4.45 times after administration of the blocking antibody (see Figure 5D).

Fluorescence Imaging of RGD-Cy5.5-MBs and Histology

For the in vitro fluorescence intensity of RGD-Cy5.5-MBs, there was no obvious difference between the ultrasound-treated group and the untreated group, indicating that the dye molecule is stable under ultrasound scanning (see Figure 6A).

According to in vivo fluorescence imaging, the fluorescence intensity of tumours increased gradually and reached a maximum 3 h after RGD-Cy5.5-MB injection (see Figure 6B). No fluorescence accumulation was observed in the tumour area in the mice of the nontargeted MB group administered Cy5.5-MBs, which were quickly cleared from the body. Additionally, fluorescence images of tissues extracted from the mice indicated that Cy5.5 fluorescence was mainly present in the kidney and liver (see Figure 6C). The fluorescence intensity in mice injected with targeted MBs was 1.8 times higher than that in mice injected with the nontargeting version (see Figure 6D).

Immunofluorescence staining of tumour sections with antibodies against αv and β3 integrin revealed that αvβ3 integrin was significantly expressed in tumour tissues (see Figure 7A). The biosafety of RGD-Cy5.5-MBs in vivo was further confirmed by HE staining of major organs (ie, heart, liver, spleen, lung, and kidney) (see Figure 7B). No histopathological damage was observed in the histopathological examination of mice treated with RGD-Cy5.5-MBs, and all of the tissue sections exhibited normal pathological morphology. The results above demonstrate that RGD-Cy5.5-MBs did not induce significant toxicity to the tissues of major organs in vivo, indicating good biocompatibility.

Conclusion

We prepared RGD peptide-targeted microbubbles for use in ultrasound and fluorescence imaging. The microbubbles were validated by examining their diagnostic effects on αvβ3 integrin-expressing tumours in MDA-MB-231 cell–bearing mice. RGD-Cy5.5-MBs exhibit excellent imaging performance and good biocompatibility in ultrasound/fluorescent imaging. This work is of importance for multimode molecular imaging for the early detection of cancer.

Funding

This project was funded by the National Natural Science Foundation of China (Grant 81760517 and 81701721) and the National Key R&D Program of China (Grant 2017YFC0112600 and 2017YFC0112603).

Disclosure

The authors declare no conflicts of interest for this work.

References

1. Anderson CR, Xiaowen H, Hua Z, et al. Ultrasound molecular imaging of tumor angiogenesis with an integrin targeted microbubble contrast agent. *Invest Radiol*. 2011;46(4):215–224.
2. Luo W, Wen G, Yang L, et al. Dual-targeted and pH-sensitive doxorubicin prodrug-microbubble complex with ultrasound for tumor treatment. *Theranostics*. 2017;7(2):452–465. doi:10.7150/thno.16677
3. Grzegorz K, Carbon JG, Grayburn PA, Fleming JB, Brekken RA. Monitoring response to anticancer therapy by targeting microbubbles to tumor vasculature. *Clin Cancer Res*. 2007;13(1):323–330. doi:10.1158/1078-0432.CCR-06-1313
4. Bloch SH, Wan M, Dayton PA, Ferrara KW. Optical observation of lipid- and polymer-shelled ultrasound microbubble contrast agents. *Appl Phys Lett*. 2004;84(4):631–633. doi:10.1063/1.1643544
5. Otani K, Nishimura H, Kamiya A, Harada-Shiba M. Simplified preparation of α v β 3 integrin targeted microbubbles based on a clinically available ultrasound contrast agent: validation in a tumor-bearing mouse model. *Ultrasound Med Biol*. 2018;44(5):1063–1073. doi:10.1016/j.ultrasmedbio.2018.01.017

6. Min HS, Kang E, Koo H, et al. Gas-generating polymeric microspheres for long-term and continuous in vivo ultrasound imaging. *Biomaterials*. 2012;33(3):936–944. doi:10.1016/j.biomaterials.2011.09.082
7. Klaus P, Robert H, Andreas O, et al. Ligand-functionalized nanoparticles target endothelial cells in retinal capillaries after systemic application. *Proc Natl Acad Sci U S A*. 2013;110(15):6115–6120. doi:10.1073/pnas.1220281110
8. Wang S, Herbst EB, Jr MF, Diakova GB, Klibanov AL, Hossack JA. Ultra-low-dose ultrasound molecular imaging for the detection of angiogenesis in a mouse murine tumor model: how little can we see? *Invest Radiol*. 2016;51(12):758–766. doi:10.1097/RLI.0000000000000310
9. Klibanov AL, Rasche PT, Hughes MS, et al. Detection of individual microbubbles of ultrasound contrast agents: imaging of free-floating and targeted bubbles. *Invest Radiol*. 2004;39(3):187–195. doi:10.1097/01.rli.0000115926.96796.75
10. Wilson SR, Burns PN. Microbubble-enhanced US in body imaging: what role? *Radiology*. 2010;257(1):24–39. doi:10.1148/radiol.10091210
11. Wang P, Yong F, Lu L, et al. NIR-II nanoprobes in-vivo assembly to improve image-guided surgery for metastatic ovarian cancer. *Nat Commun*. 2018;9(1):2898. doi:10.1038/s41467-018-05113-8
12. Claudiu-Dumitru D, Nicolae R, Doru M, Mircea C. The role of intraoperative ultrasound for the assessment of the focal liver lesions in patients with colorectal cancer. *Med Ultrason*. 2014;16(2):114–118. doi:10.11152/mu.201.3.2066.162.cdd1nr2
13. Kircher MF, Willmann JK. Molecular body imaging: MR imaging, CT, and US. part I. principles. *Radiology*. 2012;263(3):633–643. doi:10.1148/radiol.12102394
14. Kruskal JB, Kane RA. Intraoperative US of the liver: techniques and clinical applications. *Radiographics*. 2006;26(4):1067–1084. doi:10.1148/rg.264055120
15. Yue L, Chen Y, Meng D, Chen ZY. Ultrasound technology for molecular imaging: from contrast agents to multimodal imaging. *Acs Biomater Sci Eng*. 2018;4(8):2716–2728. doi:10.1021/acsbiomaterials.8b00421
16. Bachawal SV, Jensen KC, Lutz AM, et al. Earlier detection of breast cancer with ultrasound molecular imaging in a transgenic mouse model. *Cancer Res*. 2013;73(6):1689–1698. doi:10.1158/0008-5472.CAN-12-3391
17. Jaehong K, Christy C, Ah Young K, et al. In vivo NIRF and MR dual-modality imaging using glycol chitosan nanoparticles. *J Controlled Rel*. 2012;163(2):249–255. doi:10.1016/j.jconrel.2012.07.038
18. Cheung S, O'Shea DF. Directed self-assembly of fluorescence responsive nanoparticles and their use for real-time surface and cellular imaging. *Nat Commun*. 2017;8(1):1885. doi:10.1038/s41467-017-02060-8
19. Dam GM, Van George T, Crane LMA, et al. Intraoperative tumor-specific fluorescence imaging in ovarian cancer by folate receptor-α targeting: first in-human results. *Nat Med*. 2011;17(10):1315–1319. doi:10.1038/nm.2472
20. Zhen X, Xie C, Jiang Y, Ai X, Xing B, Pu K. Semiconducting photothermal nanoagonist for remote-controlled specific cancer therapy. *Nano Lett*. 2018;18(2):1498–1505. doi:10.1021/acs.nanolett.7b05292
21. Howard LP, Jonathan C, Klibanov AL, Sanjiv K, Lindner JR. Noninvasive assessment of angiogenesis by ultrasound and microbubbles targeted to alpha(v)-integrins. *Circulation*. 2003;41(6):430–431.
22. Zhang J, Feng M, Gang N, et al. 68Ga-BBN-RGD PET/CT for GRPR and Integrin αvβ3Imaging in patients with breast cancer. *Theranostics*. 2018;8(4):1121–1130. doi:10.7150/thno.22601
23. Yang J, Luo Y, Xu Y, et al. Conjugation of iron oxide nanoparticles with RGD-modified dendrimers for targeted tumor MR imaging. *ACS Appl Mater Interfaces*. 2015;7(9):5420–5428. doi:10.1021/am508983n
24. Zhu Y, Zhang J, Meng F, et al. cRGD-functionalized reduction-sensitive shell-sheddable biodegradable micelles mediate enhanced doxorubicin delivery to human glioma xenografts in vivo. *J Controlled Rel*. 2016;233:29–38. doi:10.1016/j.jconrel.2016.05.014
25. Qing-Hui Z, Ye-Zi Y, Chao W, Yi H, Cyclic DO. RGD-targeting of reversibly stabilized DNA nanoparticles enhances cell uptake and transfection in vitro. *J Drug Target*. 2009;17(5):364–373. doi:10.1080/10611860902807046
26. Fabian K, Stanley F, Patrick K, Wiltrud L, Twan L. Ultrasound microbubbles for molecular diagnosis, therapy, and theranostics. *J Nucl Med*. 2012;53(3):345–348. doi:10.2967/jnumed.111.099754
27. Daeichin V, Kooiman K, Skachkov I, et al. Quantification of endothelial αvβ3 expression with high-frequency ultrasound and targeted microbubbles: in vitro and in vivo studies. *Ultrasound Med Biol*. 2016;42(9):2283–2293. doi:10.1016/j.ultrasmedbio.2016.05.005
28. Nirupama D, Ying R, Kira F, Jarrett R, Willmann JK. Tumor angiogenic marker expression levels during tumor growth: longitudinal assessment with molecularly targeted microbubbles and US imaging. *Radiology*. 2011;258(3):804. doi:10.1148/radiol.10101079
29. Li Z, He L, He N, et al. Polymerase chain reaction coupling with magnetic nanoparticles-based biotin-avidin system for amplification of chemiluminescent detection signals of nucleic acid. *J Nanosci Nanotechnol*. 2011;11(2):1074–1078. doi:10.1166/jnn.2011.3061
30. Viswan A, Chou H, Sakudo A, Nagatsu M. Bioconjugation efficiency of plasma-functionalized carbon-encapsulated iron nanoparticles with biotin–avidin system. *Biomed Phys Eng Express*. 2015;1(4):045104. doi:10.1088/2057-1976/1/4/045104
31. Townsend SA, Evrony GD, Gu FX, Schulz MP Jr, Langer R. Tetanus toxin C fragment conjugated nanoparticles for targeted drug delivery to neurons. *Biomaterials*. 2007;28(34):5176–5184. doi:10.1016/j.biomaterials.2007.08.011
32. Zhen X, Feng X, Xie C, et al. Surface engineering of semiconducting polymer nanoparticles for amplified photoacoustic imaging. *Biomaterials*. 2017;127:97–106. doi:10.1016/j.biomaterials.2017.03.003
33. Hu Q, Wang XY, Kang LK, et al. RGD-targeted ultrasound contrast agent for longitudinal assessment of Hep-2 tumor angiogenesis in vivo. *PLoS One*. 2016;11(2):e0149075. doi:10.1371/journal.pone.0149075
34. Desgrosellier JS, Cheresh DA. Integrins in cancer: biological implications and therapeutic opportunities. *Nat Rev Cancer*. 2010;10(1):9–22. doi:10.1038/nrc2748
35. Wang J, Lu Z, Zhang J, et al. Clinical usefulness of the microbubble contrast agent sonovue in enhancing the effects of high - intensity focused ultrasound for the treatment of adenomyosis. *J Ultrasound Med off J Am Inst Ultrasound Med*. 2018;37(12):2811–2819. doi:10.1002/jum.14638
36. Li H, Yang Y, Zhang M, et al. Acoustic characterization and enhanced ultrasound imaging of long-circulating lipid-coated microbubbles. *J Ultrasound Med*. 2017;37(5):1243–1256. doi:10.1002/jum.14470